Measurement of Atmospheric Turbulence by 2-μm Doppler Lidar

IGOR SMALIKHO, FRIEDRICH KÖPP, AND STEPHAN RAHM

Institute of Atmospheric Physics, DLR, Wessling, Germany

(Manuscript received 7 September 2004, in final form 29 April 2005)

ABSTRACT

Two methods for the estimation of the turbulence energy dissipation rate (TEDR) from data measured by a 2-μm coherent Doppler lidar are described in this paper. Based on data measured at the Tarbes-Lourdes-Pyrénées International Airport in summer 2003, height profiles of TEDR have been retrieved. The results of TEDR estimation both from the Doppler spectrum width and from the velocity structure function are compared. Moreover, the experiment has been treated by numerical simulation and the theoretical results have been used for verification of the described methods.

1. Introduction

The development and employment of remote sensing devices and methods based on the Doppler effect allow new knowledge of dynamic processes in the atmosphere to be gained. Thereby, the coherent Doppler lidars have the best possibilities for such investigations in the clear atmosphere because of the high spatiotemporal resolution of the measured characteristics. These lidars are used for measurements of the wind field (Köpp et al. 1984; Hall et al. 1984; Keeler et al. 1987; Hawley et al. 1993; Frehlich et al. 1994; Banakh et al. 1995; Werner et al. 2001; Reitebuch et al. 2001; Smalikho 2003), the atmospheric turbulence (Eberhard et al. 1989; Cal-Chen et al. 1992; Gordienko et al. 1994; Smalikho 1995, 1997; Banakh and Smalikho 1997; Frehlich et al. 1998; Banakh et al. 1999; Frehlich and Cornman 2002; Davies et al. 2004), and the aircraft wake vortices (Köpp 1994, 1999; Constant et al. 1994; Hannon and Thomson 1994; Brockman et al. 1999; Harris et al. 2000, 2002; Vaughan and Harris 2001; Keane et al. 2002; Köpp et al. 2003, 2004, 2005).

The 2-μm pulsed coherent lidar (Henderson et al. 1993) has proved to be a powerful tool for wake-vortex sounding. Using this device, the lidar group of the German Aerospace Center [Deutsches Zentrum für Luft- und Raumfahrt (DLR)] carried out successful measurements of the characteristics of the wake vortices generated by large transport aircraft (Köpp et al. 2004, 2005). One of the important factors influencing the wake vortices is the atmospheric turbulence. Therefore, the extraction of information about both the wake-vortex parameters and the background wind turbulence can be helpful for the analysis of the atmospheric effect on the wake vortices. In accordance with theory (Holzäpfel et al. 2001, 2003; Gerz et al. 2002; Holzäpfel 2003; Holzäpfel and Robins 2004), the effective dwell time of the wake vortices only depends on one turbulent characteristic of the atmosphere: the turbulence energy dissipation rate (TEDR).

Several methods of TEDR estimation from data measured with a pulsed Doppler lidar are known, for example, the methods based on measurements of the spatial structure function of the wind velocity (Banakh and Smalikho 1997; Frehlich et al. 1998; Frehlich and Cornman 2002) and the width of the Doppler spectrum (Frehlich and Cornman 1999). In this paper, we describe the methods of TEDR estimation from data measured with the 2-μm pulsed Doppler lidar with laser beam scanning in a vertical plane. Such measurement geometry allows the extraction of information about both the aircraft wake vortices and the atmospheric turbulence from the lidar data only. The following two approaches are used: estimation of the TEDR from 1) the velocity structure function (VSF method) and 2) the Doppler spectrum width (DSW method). From the data measured at Tarbes, France, in summer

Corresponding author address: Friedrich Köpp, Institut für Physik der Atmosphare, DLR, Oberpfaffenhofen, D-82234 Wessling, Germany.
E-mail: friedrich.koepp@dlr.de

2003, the TEDR profiles as function of height have been retrieved. In the paper, the results obtained by these methods are compared.

2. Theory

a. Estimation of the signal power spectrum and derived parameters

The principle of pulsed Doppler lidar operation is based on the emission of laser pulses into the atmosphere and the coherent detection of the laser radiation backscattered by aerosol particles moving with the wind. The measured power of the photocurrent arising in the chain of the receiving system in the frequency range around the intermediate frequency contains the information about the speed of the moving aerosol particles in the sensing volume. An example of raw data (one shot) measured with the 2-μm pulsed Doppler lidar from DLR is shown in Köpp et al. (2004, their Fig. 2). The description of the lidar and its parameters is given by Köpp et al. (2004, 2005). The measured data are discrete with the sampling interval $T_s = 2$ ns and consists of two parts: the monitor signal $J_M^{(i)}(mT_s)$ ($m = 0, 1, 2, \ldots, m_B - 1$) and the backscatter signal (also including the noise component of the photocurrent) $J_B^{(i)}(mT_s)$ ($m = m_B, m_B + 1, m_B + 2, \ldots$), where the index i indicates the shot number and m is the sample number.

The intermediate frequency $\delta f = |f_L - f_P|$, where f_L is the frequency of the local oscillator and f_P is the frequency of the probing laser pulse, can be estimated from the power spectrum of the monitor signal. Parameters as the duration σ_p and energy U_p of the pulse and the position of the pulse center (sampling number m_0) are also estimated from the monitor signal using fast Fourier transform (FFT). For the monitor signal, the spectrum versus frequency f and the power versus time t have an almost Gaussian form. Therefore, the power of the monitor signal $P_M(t)$ can be described by the equation

$$P_M(t) = \frac{U_P}{\sqrt{\pi}\sigma_p} \exp\left(-\frac{t^2}{\sigma_p^2}\right), \tag{1}$$

and the monitor signal can be represented in the form

$$J_M^{(i)}(mT_s) = 2P_M^{1/2}(t)\cos(\Psi_0 + 2\pi\,\delta f\, t), \tag{2}$$

where $t = (m - m_0)T_s$ and Ψ_0 is a parameter equal to the phase at $t = 0$. The time dependence of Ψ_0 can be neglected. Taking into account the conditions $T_s \ll \sigma_p$ and $\sigma_p \delta f \gg 1$, and determining the monitor signal power spectrum as $S_M(f) = |\int_{-\infty}^{+\infty} dt\, J_M^{(i)}(t)\exp(-2\pi jft)|^2$, where $j = \sqrt{-1}$ and the frequency $f \in [0, (2T_s)^{-1}]$, we receive from Eqs. (1) and (2):

$$S_M(f) = \frac{U_p}{\sqrt{2\pi}\sigma_{Mf}} \exp\left[-\frac{(f - \delta f)^2}{2\sigma_{Mf}^2}\right], \tag{3}$$

where

$$\sigma_{Mf} = (\sqrt{2}\cdot 2\pi\sigma_p)^{-1} \tag{4}$$

is the width of the monitor signal power spectrum.

For estimation of the pulse energy (after calibration), the equation $U_p = 2^{-1}\int_{-\infty}^{+\infty} dt\,[J_M^{(i)}(t)]^2$ or $U_p = \int_0^{(2T_s)^{-1}} df\, S_M(f)$ can be used. The parameter σ_p can be estimated both from the measured power $\hat{P}_M(t)$ (using $\hat{\sigma}_p = \int_{-\infty}^{+\infty} dt\, \hat{P}_M(t)/[\hat{P}_M(0)\sqrt{\pi}]$) and from the measured spectrum $\hat{S}_M(f)$ (estimate $\hat{\sigma}_p$ as the second moment of the spectrum). In these two ways, practically the same estimates $\hat{\sigma}_p$ are obtained from the experimental data.

The raw data can be considered as a function of the sampling number (m), or the time after pulse emission into the atmosphere [$t = (m - m_0)T_s$], or the range ($R = ct/2$, where c is the speed of light), that is, the distance between the lidar and the center of the sensing volume. Because $T_s = 2$ ns, the sampling length $cT_s/2 = 0.3$ m. In our experiments, the minimal range for the measurement of the backscatter signal $[J_B^{(i)}(mT_s)]$ is $(m_B - m_0)T_s c/2 = 370$ m.

The velocity of the aerosol particles in the sensing volume is estimated from the power spectrum of the backscatter signal. For the sensing volume centered at the distance R from the lidar we select M samples of the backscatter signal around the sample with number $m_R = [R/(cT_s/2)] + m_0$ and multiply this array by the window function $W(m'T_s)$,

$$J_W^{(i)}(m'T_s, R) = J_B^{(i)}[(m_R - M/2 + m')T_s]W(m'T_s), \tag{5}$$

obtaining the estimate of the signal power spectrum (or Doppler spectrum)

$$\hat{S}_D^{(i)}(\Delta fk, R) = \left|\sum_{m'=0}^{M-1} J_W^{(i)}(m'T_s, R)\exp(-2\pi jkm'/M)\right|^2, \tag{6}$$

where $\Delta f = (MT_s)^{-1}$ is the width of a single frequency bin; $k = 0, 1, 2, \ldots, M/2$, and the spectral bandwidth $\Delta f M/2 \equiv (2T_s)^{-1} = 250$ MHz. The frequency resolution can be determined as $\Delta f_r = T_{\text{eff}}^{-1}$, where $T_{\text{eff}} = \int_{-\infty}^{+\infty} dt\, W(t)/W(T_s M/2)$ is the effective time of spectrum measurement. In the case of a rectangular window with M elements, $T_{\text{eff}} = MT_s$ and, therefore, $\Delta f_r = \Delta f$. Here the Gaussian window is used,

$$W(m'T_s) = \left(\frac{T_s}{\sqrt{\pi}\sigma_W}\right)^{1/2} \exp\left[-\frac{(m' - M/2)^2 T_s^2}{2\sigma_W^2}\right], \tag{7}$$

where $m' = 0, 1, 2, \ldots, M - 1$. For $T_s \ll \sigma_W \ll T_s M/2$, the effective time of spectrum measurement becomes

$$T_{\text{eff}} = \sqrt{2\pi}\sigma_W, \tag{8}$$

and therefore the frequency resolution $\Delta f_r = (\sqrt{2\pi}\sigma_W)^{-1}$. Let $\sigma_W = \sigma_p$ and $\sigma_p = 0.24$ μs (as it was in our experiments), then $\Delta f_r = 1.67$ MHz. By increasing M, Δf can be unlimitedly decreased at constant Δf_r. For the estimation of each Doppler spectrum we used $M = 2048$. In this case, the frequency bin width $\Delta f = 0.244$ MHz, and it is approximately 7 times less than Δf_r. If some points of the window are outside the data (backscatter signal), the technique of zero padding can be applied.

To decrease the fluctuations of the Doppler spectrum estimate, the method of spectral accumulation is used:

$$\tilde{S}_D(\Delta fk, R) = N_a^{-1} \sum_{i=1}^{N_a} \hat{S}_D^{(i)}(\Delta fk, R), \tag{9}$$

where N_a is the number of shots. The obtained spectra are normalized to the mean spectral noise level. This noise level is determined at frequencies outside the region of the peak containing the information about the wind velocity, after averaging a large number of realizations. The noise level can also be determined by the method described by Hildebrand and Sekhon (1974). Let $\tilde{S}_D(\Delta fk, R)$ be the normalized Doppler spectrum. Then, we select $N_{\text{ch}} = 205$ spectral channels around the mean intermediate frequency $\delta\bar{f} = N_a^{-1}\Sigma_{i=1}^{N_a}\delta f_i$. In this way, the spectral bandwidth is reduced from 250 MHz to $B = \Delta f N_{\text{ch}} = 50$ MHz.

From the measured spectra the normalized signal power $\hat{P}_S(R)$, the mean frequency $\hat{f}_D(R)$, and the square of the Doppler spectrum width $\hat{\sigma}_f^2(R)$ are estimated as zero, first, and second spectral moments, respectively,

$$\hat{P}_S(R) = \sum_{k=k_m-k_1}^{k_m+k_2} [\tilde{S}_D(\Delta fk, R) - n_{\text{th}}], \tag{10}$$

$$\hat{f}_D(R) = \hat{P}_S^{-1}(R) \sum_{k=k_m-k_1}^{k_m+k_2} \Delta fk[\tilde{S}_D(\Delta fk, R) - n_{\text{th}}], \tag{11}$$

and

$$\hat{\sigma}_f^2(R) = \hat{P}_S^{-1}(R) \sum_{k=k_m-k_1}^{k_m+k_2} [\Delta fk - \hat{f}_D(R)]^2 \times [\tilde{S}_D(\Delta fk, R) - n_{\text{th}}], \tag{12}$$

where k_1 (k_2) is the number of spectral channels [left (right)] from the channel k_m at the spectrum estimate maximum, and it is determined at the intersection point of the spectrum estimate and the selected noise threshold n_{th}. In our case, the estimate of the signal-to-noise ratio (SNR; ratio of the signal power to the mean noise power in the spectral bandwidth of 50 MHz) is given by

$$\widehat{\text{SNR}}(R) = N_{\text{ch}}^{-1}\hat{P}_s(R). \tag{13}$$

Using the Doppler equation $V = (\lambda/2)f$, where V is the radial velocity, λ is the laser wavelength, and f is the frequency shift caused by the motion of the aerosol particles, one can obtain the estimates of the radial velocity

$$\hat{V}_D(R) = (\lambda/2)[\hat{f}_D(R) - \delta\bar{f}], \tag{14}$$

and the square of the Doppler spectrum width in the velocity domain

$$\hat{\sigma}_{\text{sw}}^2(R) = (\lambda/2)^2\hat{\sigma}_f^2(R). \tag{15}$$

For estimation of $\widehat{\text{SNR}}(R)$ and $\hat{V}_D(R)$ we can chose $n_{\text{th}} = 1$ (mean noise level in the normalized spectrum). However, the noise fluctuations in the measured spectrum can be the source of large errors, when turbulent characteristics are estimated from the measured Doppler spectrum width, especially in the case of very low turbulence. To avoid the effect of these noise fluctuations we set the noise threshold above the mean noise level ($n_{\text{th}} > 1$). Concrete values for n_{th} will be determined by simulation in section 2c.

b. Estimation of turbulence parameters

The estimates $\hat{V}_D(R)$ and $\hat{\sigma}_{\text{sw}}^2(R)$ are dependent on turbulent variations of the wind. From a set of such estimates one can obtain corresponding statistical characteristics that are related to parameters of the atmospheric turbulence. The effects of spatial averaging of the radial wind velocity over the sensing volume and estimation errors resulting from backscatter signal fluctuations and noise have to be taken into account.

For the spectral accumulation 25 shots ($N_a = 25$) are used. Taking into account that the pulse repetition frequency (PRF) is 500 Hz, the measurement time of the spectrum $\tilde{S}_D(f, R)$ is $N_a/\text{PRF} = 50$ ms. During this time the distribution of the radial velocity inside the sensing volume is almost constant. In this case, it is convenient to represent the spectrum estimate in the form

$$\tilde{S}_D(f, R) = S_D(f, R) + S'_D(f, R), \tag{16}$$

where $S_D(f, R) = \langle\tilde{S}_D(f, R)\rangle_P$ is the spectrum estimate averaged over all random parameters except the radial wind velocity (conditional ensemble averaging; Frehlich 2001) and $S'_D(f, R) = \tilde{S}_D(f, R) - \langle\tilde{S}_D(f, R)\rangle_P$ are

the spectrum estimate fluctuations, $f = \Delta fk - \delta\bar{f}$. Because of the accumulation [Eq. (9)], the standard deviation of these fluctuations is approximately $\sqrt{N_a} = 5$ times less than the mean spectrum $S_D(f, R)$.

By analogy with Eq. (16), the estimates $\hat{V}_D(R)$ and $\hat{\sigma}^2_{\text{sw}}(R)$ can be represented in the form

$$\hat{V}_D(R) = V_D(R) + e(R) \tag{17}$$

and

$$\hat{\sigma}^2_{\text{sw}}(R) = \sigma^2_{\text{sw}}(R) + E(R), \tag{18}$$

where $V_D(R)$ and $\sigma^2_{\text{sw}}(R)$ are the first and second spectral moments obtained from Eqs. (10)–(15) after replacing $\tilde{S}_D(\Delta fk, R) - n_{\text{th}}$ by $S_D(f, R) - 1$ and $\Sigma_{k=k_m-k_1}^{k_m+k_2}$ Δf by $\int_{-\infty}^{\infty} df$. The second terms on the right-hand side of Eqs. (17) and (18), $e(R)$ and $E(R)$, are related to the spectrum fluctuations $S'_D(f, R)$. They will be called random errors of the estimation of $V_D(R)$ and $\sigma^2_{\text{sw}}(R)$, respectively.

From the equation for the coherently detected backscatter signal $J_B^{(i)}(t)$ (Salamitou et al. 1995; Banakh and Smalikho 1997; Frehlich 1997), the equation for the mean spectrum $S_D(f, R)$ can be obtained using conditional ensemble averaging. Then we get

$$V_D(R) = \int_{-\infty}^{+\infty} dz Q_S(z) V_r(R + z), \tag{19}$$

$$\sigma^2_{\text{sw}}(R) = \sigma_0^2 + \sigma_u^2(R), \tag{20}$$

where $V_r(z)$ is the radial wind velocity at point z, $Q_S(z)$ is the function characterizing the spatial averaging over the sensing volume, σ_0 is the spectrum width (in the velocity space) in the case of $V_r(z) = \text{constant}$, and

$$\sigma_u^2(R) = \int_{-\infty}^{+\infty} dz Q_S(z)[V_r(R + z) - V_D(R)]^2 \tag{21}$$

is the term related to the inhomogeneity of the wind field inside the sensing volume. In our case of the Gaussian pulse and window [see Eqs. (1), (7)], the function $Q_S(z)$ also has a Gaussian shape:

$$Q_S(z) = \Delta z^{-1} \exp(-\pi z^2/\Delta z^2), \tag{22}$$

where

$$\Delta z = \sqrt{\pi}\sqrt{\sigma_p^2 + \sigma_W^2}(c/2) \tag{23}$$

is the longitudinal size of the sensing volume, and σ_0^2 is described by the equation

$$\sigma_0^2 = (\lambda/2)^2[\sigma_{Mf}^2 + (8\pi^2\sigma_W^2)^{-1} + \sigma_\delta^2]. \tag{24}$$

In Eq. (24) we take into account the spectral broadening resulting from the probing pulse (first term in square brackets), the window effect (second term), and the variance of the intermediate frequency (third term).

Let us represent the radial velocity in the form $V_r(z) = \langle V_r(z)\rangle + V'_r(z)$, where the angular brackets stand for ensemble averaging and $V'_r = V_r - \langle V_r\rangle$ are fluctuations. For the case of wind shear we assume that in the interval $[R - \Delta z/2, R + \Delta z/2]$ the mean velocity can be described by the equation

$$\langle V_r(R + z)\rangle = \langle V_r(R)\rangle + \mu(R)z, \tag{25}$$

where $\mu = d\langle V_r\rangle/dz$. By substitution of Eq. (25) into Eq. (19) and averaging, we find $\langle V_D(R)\rangle = \langle V_r(R)\rangle$. From Eqs. (21) and (25) we obtain

$$\langle\sigma_u^2\rangle = \sigma_s^2 + \sigma_t^2, \tag{26}$$

where

$$\sigma_s^2 = (2\pi)^{-1}(\mu\Delta z)^2 \tag{27}$$

and

$$\sigma_t^2 = \int_{-\infty}^{+\infty} dz Q_S(z)\langle[V'_r(R + z) - V'_D(R)]^2\rangle \tag{28}$$

are terms related to the spectral broadening resulting from wind shear (σ_s^2) and turbulence (σ_t^2); $V'_D = V_D - \langle V_D\rangle$.

The spatial structure of the turbulence is described by characteristics like the structure function $D_V(r)$, variance σ_V^2, correlation function $B_V(r)$, and spectrum $S_V(\kappa)$ of the wind velocity fluctuations. For the case of radial wind velocity and homogeneous turbulence $D_v(r)$ and $B_v(r)$ can be written as

$$D_V(r) = \langle[V'_r(z_1 + r) - V'_r(z_1)]^2\rangle = 2[\sigma_V^2 - B_V(r)], \tag{29}$$

$$B_V(r) = \langle V'_r(z_1 + r)V'_r(z_1)\rangle = 2\int_0^\infty d\kappa S_V(\kappa)\cos(2\pi\kappa r), \tag{30}$$

where $\sigma_V^2 = \langle(V'_r)^2\rangle = B_V(0)$.

In the inertial subinterval of the turbulence ($L_\eta \ll r \ll L_V$ or $L_\eta^{-1} \gg \kappa \gg L_V^{-1}$, where L_η is the inner scale of turbulence and L_V is the integral scale of turbulence), the structure function and the spectrum of wind velocity are only depending on the TEDR ε. They are described by the Kolmogorov law (Lumley and Panofsky 1964; Monin and Yaglom 1975)

$$D_V(r) = C_K\varepsilon^{2/3}r^{2/3}, \tag{31}$$

$$S_V(\kappa) = 0.0365C_K\varepsilon^{2/3}\kappa^{-5/3}, \tag{32}$$

where $C_K \approx 2$ is the Kolmogorov constant.

There are many spectral models describing the full range of turbulent inhomogeneities of the wind, in par-

ticular, the von Kármán model (Lumley and Panofsky 1964; Vinnichenko et al. 1973),

$$S_V(\kappa) = 2\sigma_V^2 L_V[1 + (8.42 L_V\kappa)^2]^{-5/6}, \quad (33)$$

where the integral scale of turbulence L_V is determined as

$$L_V = \int_0^\infty dr B_V(r)/\sigma_V^2, \quad (34)$$

which is proportional to the outer scale of turbulence $L_o = 1.34 L_V$ (Frehlich 1997).

From Eqs. (32) and (33) we have

$$\varepsilon = \frac{1.972}{C_K^{3/2}} \frac{\sigma_V^3}{L_V}. \quad (35)$$

In the case of homogeneous turbulence at very large separation $r \to \infty$, the structure function reaches the saturation: $D_V(\infty) = 2\,\sigma_V^2$.

In Eq. (17), $V_D(R)$ and $e(R)$ are statistically independent (Frehlich 2001). Then we obtain the variance and the structure function of the radial velocity of Doppler lidar estimate:

$$\sigma_{\hat{V}_D}^2 = \sigma_{V_D}^2 + \sigma_e^2 \quad (36)$$

and

$$D_{\hat{V}_D}(r) = D_{V_D}(r) + D_e(r), \quad (37)$$

where $\sigma_{V_D}^2 = \langle (V_D')^2 \rangle$, $\sigma_e^2 = \langle e^2 \rangle$ (for unbiased estimate $\langle e \rangle = 0$), $D_{V_D}(r) = \langle [V_D'(R + r) - V_D'(R)]^2 \rangle$, and $D_e(r) = \langle [e(R + r) - e(R)]^2 \rangle$. In accordance with Eqs. (18), (20), and (26), the mean square of the Doppler spectrum width is determined as

$$\langle \hat{\sigma}_{\text{sw}}^2 \rangle = \sigma_0^2 + \sigma_s^2 + \sigma_t^2 + \langle E \rangle. \quad (38)$$

From Eqs. (19), (29), (30), (33), and (35) we obtain

$$\sigma_V^2 = \sigma_{V_D}^2 + \sigma_t^2, \quad (39)$$

$$D_{V_D}(r) = \varepsilon^{2/3} G_S(r, \Delta z, L_V), \quad (40)$$

where

$$G_S(r, \Delta z, L_V) = 0.497 C_K r^{2/3} \int_0^\infty \frac{d\xi (1 - \cos\xi) \exp[-(\xi \Delta z/r)^2/(2\pi)]}{[\xi^2 + (0.746 r/L_V)^2]^{5/6}}, \quad (40a)$$

and

$$\sigma_t^2 = \varepsilon^{2/3} G_W(\Delta z, L_V), \quad (41)$$

where

$$G_W(\Delta z, L_V) = 0.2485 C_K \Delta z^{2/3} \int_0^\infty \frac{d\xi \{1 - \exp[-\xi^2/(2\pi)]\}}{[\xi^2 + (0.746 \Delta z/L_V)^2]^{5/6}}. \quad (41a)$$

According to Eqs. (35) and (41), the ratio σ_t^2/σ_V^2 is a function of the ratio $L_V/\Delta z$,

$$\sigma_t^2/\sigma_V^2 = F_W(L_V/\Delta z), \quad (42)$$

where $F_W(L_V/\Delta z) = (1.972)^{2/3} C_K^{-1} L_V^{-2/3} G_W(\Delta z, L_V)$.

On the basis of the obtained equations it is possible to develop two methods of TEDR estimation from the measured lidar data.

1) The method of TEDR estimation from the velocity structure function (VSF method) is described.

   This method has been described in detail by Frehlich and Cornman (2002). From the measured data, the estimates of the structure functions $\hat{D}_{\hat{V}_D}(i\Delta r)$ and $\hat{D}_e(i\Delta r)$ can be derived. The measured difference $\hat{D}_{\hat{V}_D}(i\Delta r) - \hat{D}_e(i\Delta r)$ is fitted to the function $D_{V_D}(i\Delta r)$ given by Eq. (40), in order to find ε and L_V in such a way that the best fitting takes place for both variables. The turbulent parameters (estimates $\hat{\varepsilon}$ and $\hat{L}_V$) are determined by minimizing the functional (Frehlich and Cornman 2002)

$$\rho(\varepsilon, L_V) = \sum_{i=1}^{I} i^{-2} [\gamma(i\Delta r, L_V) - \varepsilon^{2/3}]^2, \quad (43)$$

   where

$$\gamma(i\Delta r, L_V) = \frac{\hat{D}_{\hat{V}_D}(i\Delta r) - \hat{D}_e(i\Delta r)}{G_S(i\Delta r, \Delta z, L_V)}. \quad (44)$$

   This algorithm is used with values of $\Delta r = 30$ m and $I = 16$.

2) The method of TEDR estimation from the Doppler spectrum width (DSW method) is described.

   Knowing the parameters σ_0^2, σ_s^2 and $\langle E \rangle$, and using Eq. (38) and the measured mean square of the spectrum width $\langle \hat{\sigma}_{\text{sw}}^2 \rangle_E$, one can estimate the mean turbulent broadening of the spectrum as

$$\hat{\sigma}_t^2 = \langle \hat{\sigma}_{\text{sw}}^2 \rangle_E - \sigma_0^2 - \sigma_s^2 - \langle E \rangle, \quad (45)$$

   where $\langle x \rangle_E$ denotes the estimate of the mean value $\langle x \rangle$. The measurement results of the variances $\hat{\sigma}_{\hat{V}_D}^2$

and $\hat{\sigma}_e^2$ allow the estimate of the radial velocity variance to be obtained [see Eqs. (36) and (39)]:

$$\hat{\sigma}_V^2 = \hat{\sigma}_{\hat{V}_D}^2 - \hat{\sigma}_e^2 + \hat{\sigma}_t^2. \quad (46)$$

Using the ratio $\hat{\sigma}_t^2/\hat{\sigma}_V^2$ and Eq. (42), the integral scale of turbulence $\hat{L}_V$ can be determined. When $\hat{\sigma}_V^2$ and $\hat{L}_V$ are known, the estimate $\hat{\varepsilon}$ can be calculated by Eq. (35).

Information about σ_0^2 is extracted from the data of the monitor signal [see Eqs. (3) and (24)], and σ_s^2 can be found by using Eq. (27). Only the parameter $\langle E\rangle$ in Eq. (45) is not determined. If the noise threshold is set to $n_{\text{th}} = 1$ for the estimation of the second moment in Eq. (12), then $\langle E\rangle \neq 0$. Although at SNR ≥ 1 this error $\langle E\rangle \ll \sigma_0^2$, we cannot neglect it in Eq. (45), especially in the case of weak turbulence. In our work, we select the noise threshold n_{th} for minimization of the error $\langle E\rangle$ [when we can neglect $\langle E\rangle$ in Eq. (45)] on the basis of numerical simulation results.

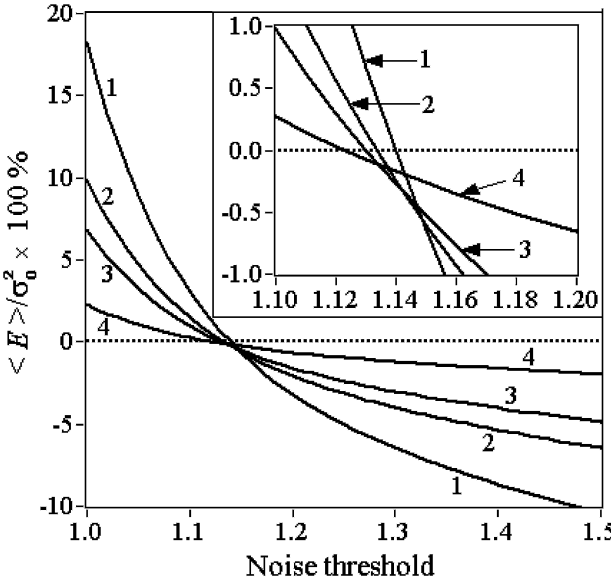

FIG. 1. Error of the estimation of the mean square of the Doppler spectrum width vs noise threshold at SNR = 1 (curve 1), 2 (curve 2), 3 (curve 3), and 10 (curve 4).

c. Numerical simulation

For the computer simulation of random realizations of the backscatter signal $J_B^{(i)}(mT_s)$ (Banakh and Smalikho 1997; Frehlich 1997) and simulated data processing, the following parameters were used: $\sigma_p = \sigma_W = 0.2488\ \mu$s, $\sigma_\delta = 0.1$ MHz (i.e., $\sigma_0 \approx 0.647\ \text{m s}^{-1}$ and $\Delta z \approx 94$ m), and $N_a = 25$. Applying the processing procedures given in section 2a, we obtained the estimates $\hat{V}_D(R)$ and $\hat{\sigma}_{\text{sw}}^2(R)$. In the beginning, lidar signals for the case of homogeneous wind [$V_r(z)$ = constant or $\varepsilon = 0$] were simulated, and estimates of $\hat{\sigma}_{\text{sw}}^2(R)$ at various noise thresholds n_{th}were obtained. Then, the error $\langle E\rangle = \langle\hat{\sigma}_{\text{sw}}^2\rangle - \sigma_0^2$ as a function of n_{th} was calculated. Figure 1 shows the normalized estimation error of the mean square of the Doppler spectrum width versus the noise threshold at different SNR. The intersection of the curves with the zero level (dashed line) occurs in the interval of $1.12 < n_{\text{th}} < 1.14$. The optimal noise threshold $n_{\text{th}}^{\text{opt}}$, determined as $\langle E(n_{\text{th}}^{\text{opt}})\rangle = 0$, at fixed N_a is a function of the SNR. Using this optimal threshold for the estimation of the second spectral moment, $\langle E\rangle$ can be neglected in Eq. (45).

On the basis of the numerical simulation results, the accuracy of TEDR estimation by the VSF and DSW methods were investigated. As in the paper of Frehlich and Cornman (2002), the lidar signals were simulated for the case of a laser beam pointing at a fixed elevation angle and frozen homogeneous velocity field, which is moving in the direction perpendicular to the beam with a mean velocity of 3 m s^{-1}. For the simulation of 2D wind field realizations, we assumed isotropic turbulence and used the von Kármán model for a 2D velocity spectrum with $L_V = 150$ m and various ε. The parameters $\hat{V}_D(R_k)$ and $\hat{\sigma}_{\text{sw}}^2(R_k)$ are estimated at ranges $R_k = R_0 + (k-1)\Delta R$, where $k = 1, 2, \ldots, 40$, $\Delta R = 30$ m. For agreement with the conditions of the real experiment, as described in section 3, we assume that the estimates $\hat{V}_D(R_k)$ and $\hat{\sigma}_{\text{sw}}^2(R_k)$ are obtained every 0.5 s, resulting in $40 \times 600 = 24\,000$ estimates within a period of 5 min. We also take into account the range dependence of the SNR observed on the first day of the experiment (see Fig. 5a), whereby the maximum and minimum SNR equals 3 and 1, respectively. Using 24 000 estimates of $\hat{V}_D(R_k)[\hat{\sigma}_{\text{sw}}^2(R_k)]$, the TEDR was determined by the VSF (DSW) method described in section 2b. In the case of the DSW method, the estimates $\hat{\sigma}_{\text{sw}}^2(R_k)$ were obtained on the basis of the calculated dependence of $n_{\text{th}}^{\text{opt}}$ versus SNR, and at a fixed noise threshold of $n_{\text{th}} = 1.14$ (optimal for SNR = 1) and $n_{\text{th}} = 1.13$ (optimal for SNR = 3).

Assuming that $\hat{\varepsilon}_1$ and $\hat{\varepsilon}_2$ are TEDR estimates obtained by the VSF ($\hat{\varepsilon}_1$) and DSW ($\hat{\varepsilon}_2$) methods from the same simulated (measured) lidar data, the data for different true TEDR ε was simulated. For each ε value, 500 independent estimates for $\hat{\varepsilon}_1$ and $\hat{\varepsilon}_2$ were used for the statistical analysis of the results. The following statistical characteristics of TEDR estimation were calculated: the relative bias

$$b = (\langle\hat{\varepsilon}\rangle/\varepsilon - 1) \times 100\%, \quad (47)$$

the relative error

$$\mathrm{Err} = [\langle(\hat{\varepsilon}/\varepsilon - 1)^2\rangle]^{1/2} \times 100\%, \quad (48)$$

and the discrepancy parameter of TEDR estimates by VSF and DSW methods

$$d = 2[\langle(\hat{\varepsilon}_1 - \hat{\varepsilon}_2)^2/(\hat{\varepsilon}_1 + \hat{\varepsilon}_2)^2\rangle]^{1/2} \times 100\%. \quad (49)$$

Figure 2 shows results for the relative bias of TEDR estimation by the VSF (circles) and DSW (squares) methods. It can be seen that the VSF estimator gives a small bias (less than 3%) for any turbulence strength. There is also an insignificant bias for the case of the DSW method, when the optimal noise threshold $n_{\mathrm{th}}^{\mathrm{opt}}$ is used (squares connected by solid lines). However, a relatively small deviation of the noise threshold from the optimal one can produce a large bias of the TEDR estimation, especially in the case of weak turbulence TEDR $< 10^{-4}\mathrm{m}^2\,\mathrm{s}^{-3}$. There is an overestimation for $n_{\mathrm{th}} = 1.13$ (curve 1) and an underestimation for $n_{\mathrm{th}} = 1.14$ (curve 2).

The relative errors of TEDR estimation by the VSF (full circles) and DSW (squares) methods are shown in Fig. 3. In the case of the DSW estimator, only the optimal noise threshold $n_{\mathrm{th}}^{\mathrm{opt}}$ was used. It can be seen that the relative error of the TEDR estimation from the velocity structure function is almost constant for any TEDR $\in [10^{-5}-10^{-2}]$ $\mathrm{m}^2\,\mathrm{s}^{-3}$, and equals approximately 20%. At $\varepsilon > 10^{-4}\mathrm{m}^2\,\mathrm{s}^{-3}$, the error of the TEDR estimation by DSW (~10%) is approximately 2 times less than that in the case of the VSF method. It is interesting to note that the standard deviation of $\sigma_u^2(R)$ [see Eq. (21)] is also 2 times less than the standard deviation of the velocity difference square $[V_D(R + r) - V_D(R)]^2$, where $r = 30$ m. Moreover, Fig. 3 shows the results for the discrepancy parameter d (circles connected by dashed lines). The same parameter can be calculated from the data of the real experiment. The results of the discrepancy parameter d for both the numerical simulation and the field experiment will be compared in section 3.

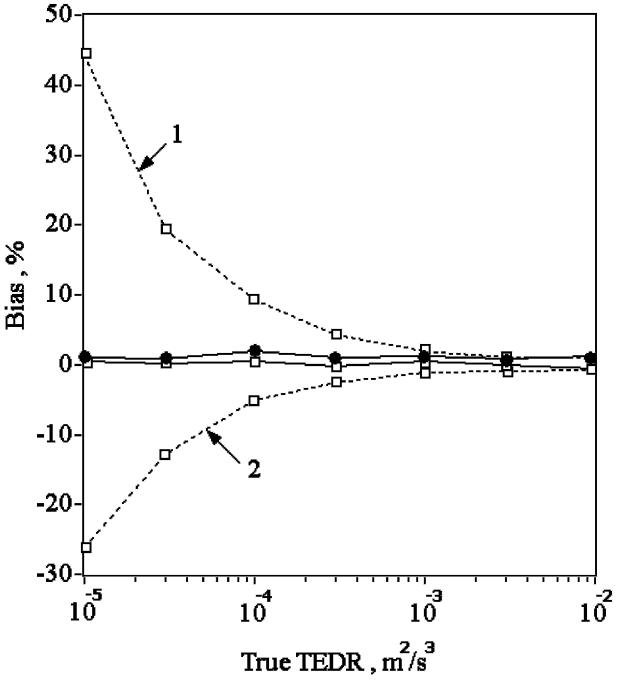

FIG. 2. Bias of TEDR estimates obtained by VSF (circles) and DSW (squares) at optimal noise threshold (squares connected by solid lines), and at $n_{\mathrm{th}} = 1.13$ (curve 1) and $n_{\mathrm{th}} = 1.14$ (curve 2).

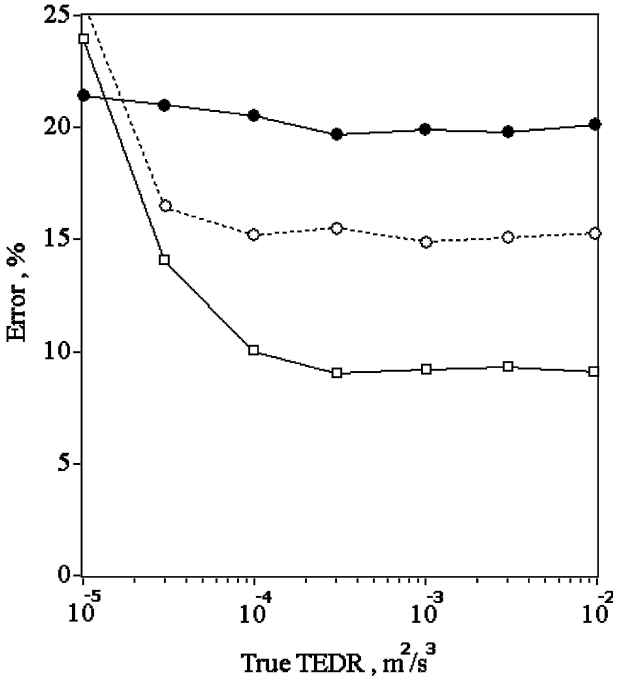

FIG. 3. Relative error of TEDR estimation by VSF (full circles) and DSW (squares) methods and the discrepancy parameter d (open circles connected by dashed lines).

3. Experiment

a. Measurement and data processing

In summer 2003, the lidar group of DLR carried out measurements with the 2-μm pulsed Doppler lidar at the airfield of the Tarbes-Lourdes-Pyrénées International Airport in France, in the frame of the European Community (EC) Aircraft Wing with Advanced Technology Operation (AWIATOR) project. One of the main tasks of this project was the experimental investigation of wake vortices generated by a large transport aircraft. This experiment offered the possibility to si-

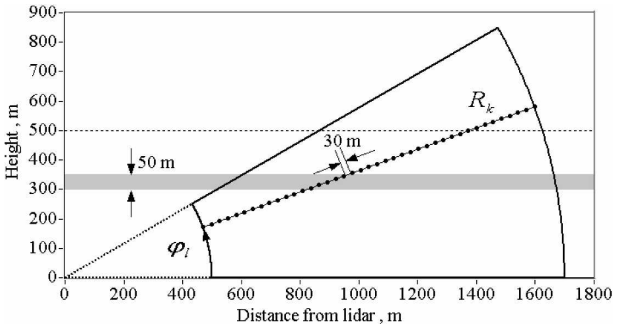

FIG. 4. Measurement geometry.

multaneously measure the atmospheric turbulence and the wake-vortex behavior. The measurements were carried out on 2 days: 27 and 28 August. The lidar worked continuously during the following intervals: 1200–1216, 1300–1316, 1800–2020 (27 August), and 0806–1015 (28 August) local time (LT). The weather conditions favored the success of this experiment because of the rather high concentration of aerosol particles in the atmosphere and fine weather (except for the first 30 min of measurements on 28 August, when the maximum height of probing ~600 m was determined by the lower bound of clouds).

The measurement geometry is sketched in Fig. 4. The laser beam was scanned in the vertical plane by turning up and down with an angular speed of $2^0\ s^{-1}$. The minimum and maximum of the elevation angle φ was 0^0 and 30^0, respectively ($0^0 \le \varphi \le 30^0$). The main parameters of the lidar and the data processing are summarized in Table 1.

From the measured data the Doppler spectra $\tilde{S}_D(f, R)$ were estimated at ranges of $R_k = R_0 + k\Delta R$, where $R_0 = 500$ m; $\Delta R = 30$ m; $k = 0, 1, 2, \ldots, K - 1$; and $K = 40$; and at elevation angles $\varphi_l = l\Delta\varphi$, where $l = 0, 1, 2, \ldots, 300$, $\Delta\varphi = 0.1^0$ ($d\varphi/dt = 2^0\ s^{-1}$, PRF = 500 Hz, $N_a = 25$). Using the estimation algorithms described by Eqs. (10)–(15), we obtained a set of data for the signal-to-noise ratio $\widehat{\mathrm{SNR}}(R_k, \varphi_l, n) \equiv \widehat{\mathrm{SNR}}(h_{kl}, n)$, the radial wind velocity $\hat{V}_D(R_k, \varphi_l, n) \equiv \hat{V}_D(h_{kl}, n)$, and the square of the Doppler spectrum width $\hat{\sigma}^2_{\mathrm{sw}}(R_k, \varphi_l, n) \equiv \sigma^2_{\mathrm{sw}}(h_{kl}, n)$, where $h_{kl} = R_k \sin\varphi_l$ is the height and $n = 1, 2, 3, \ldots$ is the scan number.

The mean signal-to-noise ratio was estimated as

$$\widehat{\mathrm{SNR}}(R_k, \varphi_l) = N_s^{-1} \sum_{n=1}^{N_s} \widehat{\mathrm{SNR}}(R_k, \varphi_l, n), \qquad (50)$$

where N_s is the number of scans of the laser beam during the measurement of the data used for averaging.

Assuming that the mean horizontal wind component in the plane formed by the scanning laser beam (or crosswind velocity) $\langle V_c \rangle = \langle V_r \rangle / \cos\varphi = \langle \hat{V}_D \rangle / \cos\varphi$ is only depending on the height h, at first we find an estimate for this characteristic as

$$\langle V_c(h) \rangle_E = (N_s L)^{-1} \sum_{n=1}^{N_s} \sum_{h-\delta < h_{kl} < h+\delta}^{L} \hat{V}_D(h_{kl}, n)(\cos\varphi_l)^{-1}, \qquad (51)$$

where, in addition to averaging over the number of scans N_s, we average all estimates $\hat{V}_D / \cos\varphi_l$ that are inside the layer of thickness $\Delta h = 2\delta = 50$ m (shown in Fig. 4 as a gray band), and L is the number of estimates in this layer during one scan. Then, the 2D distribution of the mean radial velocity can be calculated by

$$\langle V_D(R_k, \varphi_l) \rangle_E \equiv \langle V_D(h_{kl}) \rangle_E = \langle V_c(h_{kl}) \rangle_E \cos\varphi_l. \qquad (52)$$

TABLE 1. Main parameters of the 2-μm coherent Doppler lidar.

Slave laser (Tm:LuAG)	Wavelength	2022.54 nm
	Pulse energy	2.0 mJ
	Pulse length [full-width half maximum (FWHM)]	400 ± 40 ns
	Pulse repetition rate	500 Hz
	Master laser/slave laser frequency offset	102 ± 3 MHz
Telescope	Off-axis type	
	Aperture	108 mm
Scanner	Oscillating mirror	
	Vertical scan range	0°–30°
	Scan duration	15 s
Data acquisition	Concept of early digitizing	
	Sampling rate	500 MHz
	Sample length	0.3 m
Measurement range	Processed data	500–1700 m
Doppler spectra sampling	Along line of sight (LOS)	30 m
	Perpendicular to LOS	1–4 m

Using the resulting estimates $\langle V_D(R_k, \varphi_l)\rangle_E$, we calculate the fluctuations $\hat{V}'_D(R_k, \varphi_l, n) \equiv \hat{V}'_D(h_{kl}, n) = \hat{V}_D(R_k, \varphi_l, n) - \langle V_D(R_k, \varphi_l)\rangle_E$ and the parameter

$$\hat{\mu}(R_k, \varphi_l) \equiv \hat{\mu}(h_{kl}) = [\langle V_D(R_{k+1}, \varphi_l)\rangle_E - \langle V_D(R_{k-1}, \varphi_l)\rangle_E]/(2\Delta R). \quad (53)$$

In accordance with Eq. (45), where we take $\langle E\rangle = 0$, the mean turbulent broadening of the Doppler spectrum is estimated, using the equation

$$\hat{\sigma}_t^2(h) = (N_s L)^{-1} \sum_{n=1}^{N_s} \sum_{h-\delta<h_{kl}<h+\delta}^{L} [\hat{\sigma}_{\rm sw}^2(h_{kl}, n) - \hat{\mu}^2(h_{kl})\Delta z^2 (2\pi)^{-1} - \sigma_0^2(\varphi_l, n)]. \quad (54)$$

The statistical characteristics of the velocity estimation error $e(R)$ can be determined by the known methods (Frehlich 2001). From the velocities measured with the Doppler lidar we obtain the differences

$$\hat{e}(R_k, \varphi_l, n) = [\hat{V}_D(R_k, \varphi_{l+1}, n) - \hat{V}_D(R_k, \varphi_l, n)]/\sqrt{2}, \quad (55)$$

which are used for estimation of the variance

$$\hat{\sigma}_e^2(h) = (N_s L)^{-1} \sum_{n=1}^{N_s} \sum_{h-\delta<h_{kl}<h+\delta}^{L} \hat{e}^2(h_{kl}, n). \quad (56)$$

On the basis of Eq. (46), an estimate of the wind velocity variance $\hat{\sigma}_V^2(h)$ is calculated by the equation

$$\hat{\sigma}_V^2(h) = (N_s L)^{-1} \sum_{n=1}^{N_s} \sum_{h-\delta<h_{kl}<h+\delta}^{L} [\hat{V}'_D(h_{kl}, n)]^2 - \hat{\sigma}_e^2(h) + \hat{\sigma}_t^2(h), \quad (57)$$

assuming homogeneous and isotropic turbulence within the layer of 50 m thickness.

For estimation of the velocity structure function $\hat{D}_{\hat{V}_D}(r_i, h)$ and $\hat{D}_e(r_i, h)$, at first, the squares of the velocity difference $\tilde{D}_{\hat{V}_D}(r_i, h_{kli}, n) = [\hat{V}'_D(R_k + r_i, \varphi_l, n) - \hat{V}'_D(R_k, \varphi_l, n)]^2$ and $\tilde{D}_e(r_i, h_{kli}, n) = [\hat{e}(R_k + r_i, \varphi_l, n) - \hat{e}(R_k, \varphi_l, n)]^2$ are obtained, where $r_i = i\Delta R$, $i = 1, 2, \ldots, 16$, and $h_{kli} = (R_k + r_i/2)\sin\varphi_l$. Then, we use the equations

$$\hat{D}_{\hat{V}_D}(r_i, h) = (N_s L)^{-1} \sum_{n=1}^{N_s} \sum_{h-\delta<h_{kli}<h+\delta}^{L} \tilde{D}_{\hat{V}_D}(r_i, h_{kli}, n), \quad (58)$$

$$\hat{D}_e(r_i, h) = (N_s L)^{-1} \sum_{n=1}^{N_s} \sum_{h-\delta<h_{kli}<h+\delta}^{L} \tilde{D}_e(r_i, h_{kli}, n). \quad (59)$$

During the measurement periods, every 8–10 min an overflight of the large transport aircraft at approximately a 300-m height in the plane perpendicular to the scanning plane occurred. After each overflight the effect of the wake vortices on the measured data could be observed for several minutes. For TEDR determination, the data measured in the vicinity of the vortices have been excluded.

The mean square of the Doppler spectrum width and the velocity structure function was estimated at different heights every 50 m, from $h = 50$ m to $h = 500$ m for data measured on 27 August, and $h = 300$ m for data measured on 28 August.

Figure 5 shows two examples of measured SNR versus range R at $\varphi = 2^0$ (solid curve) and $\varphi = 28^0$. To increase the SNR in the region where wake vortices are expected ($R \sim 0.5$–1 km), the laser beam was focused on an approximately 1-km range. This allowed for a 5-times increase of the SNR in the region of 0.5 km $\leq R \leq 1$ km, but at a range of $R \sim 3$ km the SNR was 2 times less as compared with that of the case of a collimated beam. For processing, we used measured data at ranges up to $R = 1700$ m. In this case, the condition SNR ≥ 1 is valid for all data measured up to the maximal height of $h = 500$ m. The second spectral moments were estimated at the optimal noise threshold $n_{\rm th}^{\rm opt}$ as a function of SNR in accordance with the result of numerical simulation. In our experiment $1 \leq$ SNR ≤ 20 and $1.12 < n_{\rm th}^{\rm opt} < 1.14$.

b. Measurement results

For retrieving the TEDR height profiles the two approaches described in section 2—the estimation of TEDR from 1) the VSF and 2) the DSW methods—were used. To investigate the influence of turbulence on the aircraft wake vortices, we retrieved the height profiles of TEDR from lidar data measured during 20 scans. In accordance with the results of numerical simulation, this measurement period of 5 min should be optimal, because the level of statistical uncertainty is relatively low (see Fig. 3) and the period between aircraft overflights is ~8–10 min. Moreover, the dwell time of the wake vortices generated by the large transport aircraft is less than 5 min.

Figures 6 and 7 show examples of height profiles for the TEDR (Figs. 6a and 7a) and integral scale of turbulence (Figs. 6b and 7b) retrieved by the two methods: VSF (circles) and DSW (squares). The results of the

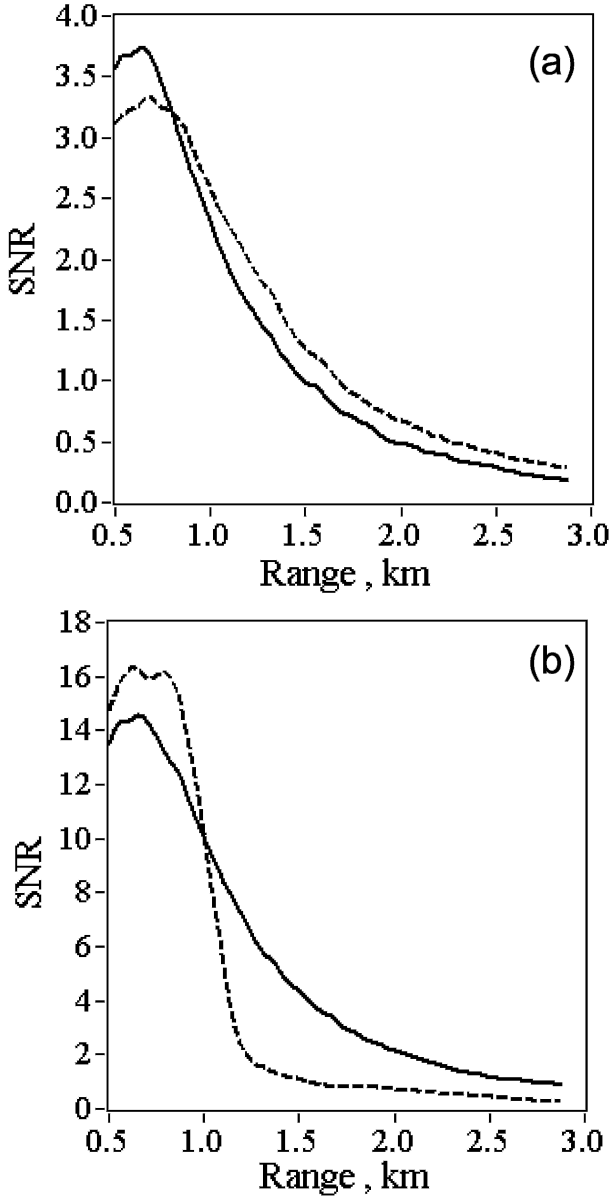

FIG. 5. SNR vs range at elevation angle 2^0 (solid curves) and 28^0 (dashed curves). The curves show the results of 30-min measurements on (a) 27 Aug 2003 and (b) 28 Aug 2003.

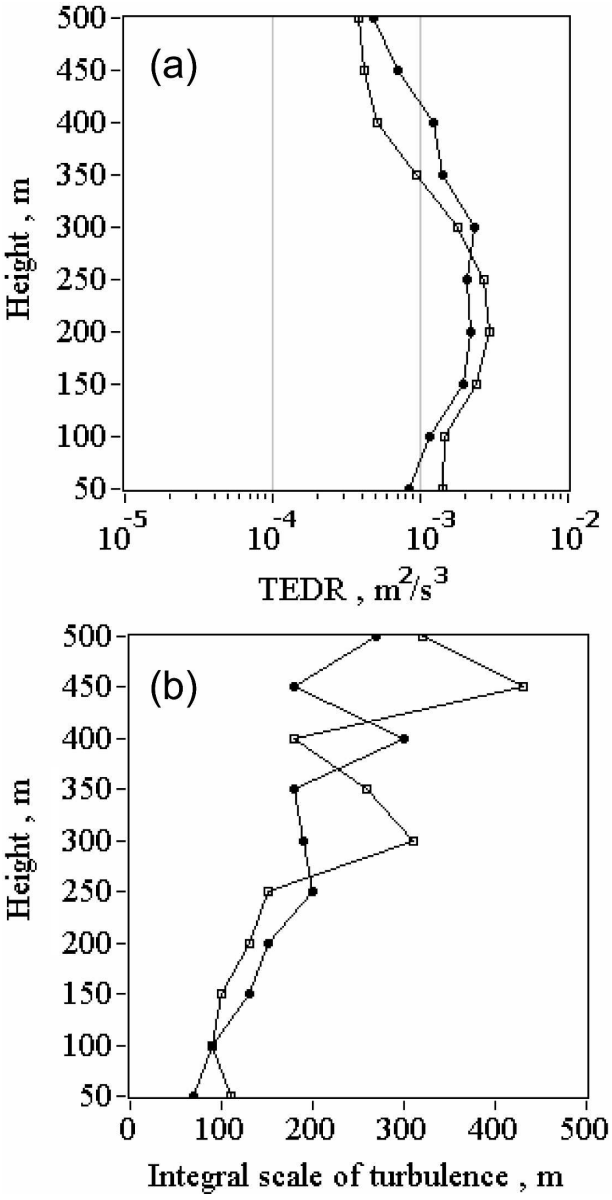

FIG. 6. Example of height profiles of (a) TEDR and (b) the integral scale of turbulence retrieved by VSF (circles) and DSW (squares) method from data measured at 1204:24–1209:49 LT 27 Aug 2003.

measurements at noon (Fig. 6) and in the evening (Fig. 7) of 27 August are presented. In the beginning of the measurement on 28 August, clouds were above a height of ~500–600 m and, therefore, the TEDR profile retrieval is limited to this height. Then, within approximately half an hour, the clouds lifted and at heights above ~400 m a jet flow with strong wind shear came up. The attempt to take into account the inhomogeneity of the mean wind [using Eqs. (48)–(50)] in the vicinity of the jet flow was not successful, because the jet flow height changed slowly during 5 min of measurement (mesoscale wind variations), resulting in too "smoothed" profiles of the mean radial velocity. As a result, the TEDR obtained by both methods is overestimated. Therefore, from data measured on 28 August, the retrieved height profiles of TEDR were limited to heights below 300 m.

In Fig. 8, the TEDR versus time at a height $h = 200$ m for measurements on 27 (Fig. 8a) and 28 (Fig. 8b) August is shown. In case (Fig. 8a), the TEDR decreased during the time period of 1800–1950 LT, then it

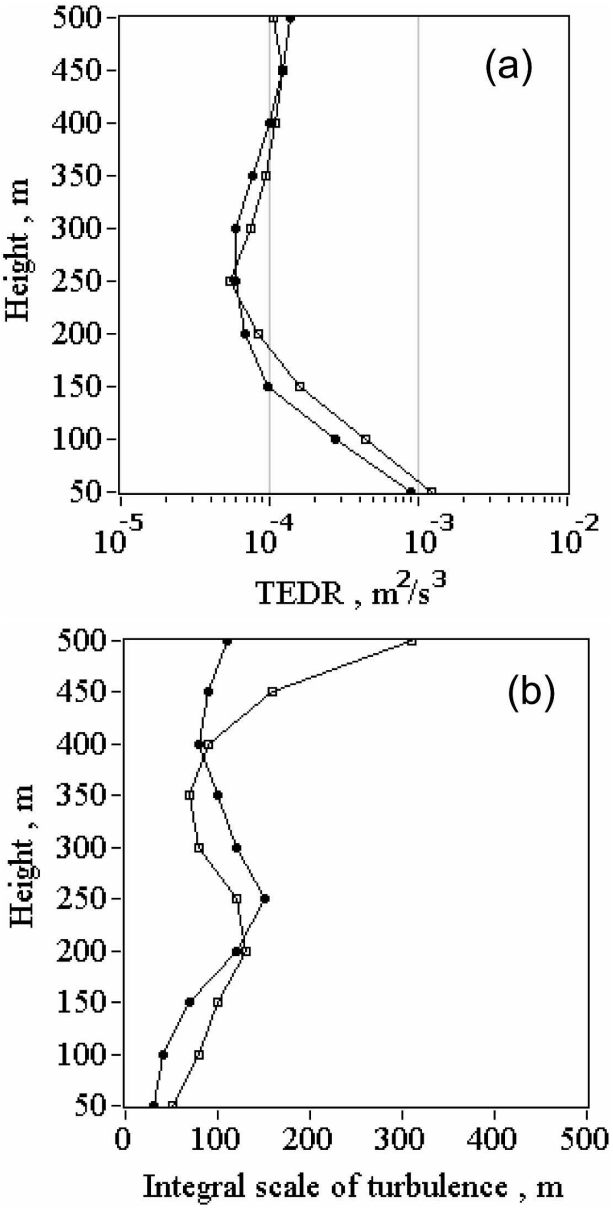

FIG. 7. Example of height profiles of (a) TEDR and (b) the integral scale of turbulence retrieved by VSF (circles) and DSW (squares) method from data measured at 1729:08–1734:42 LT on 27 Aug 2003.

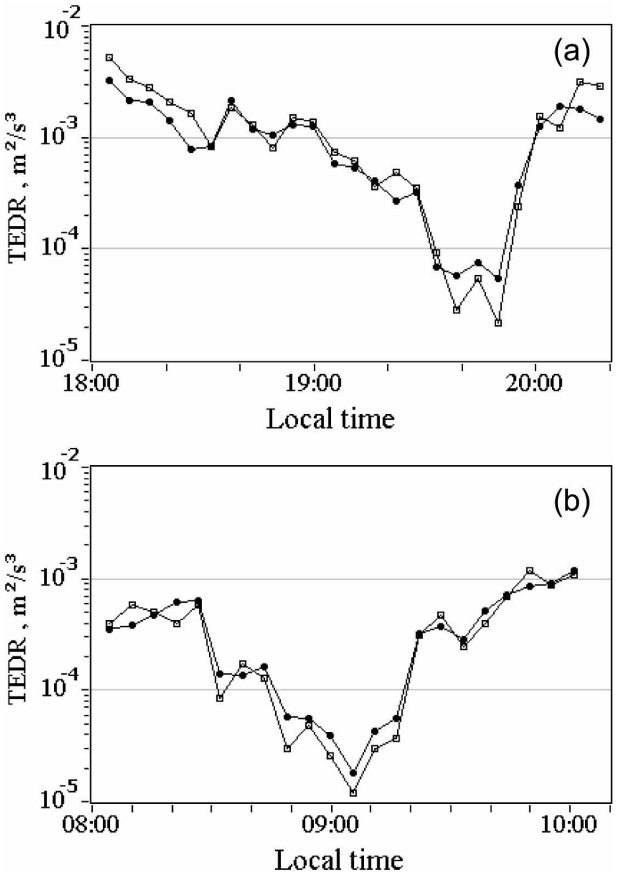

FIG. 8. TEDR vs time at a height of 200 m. The data were measured on (a) 27 and (b) 28 Aug. The TEDR estimates are obtained from VSF (circles) and from DSW methods (squares).

increased very quickly. The reason for this behavior is a wind front coming into the measurement region. Within 10 min, the crosswind velocity V_c increased from ~1 up to ~10 m s^{-1}. On the next day (Fig. 8b), after approximately 0920 LT, the TEDR increased at an almost constant wind velocity of ~2 m s^{-1}. In this time, the sun heated the earth's surface and the thermal stratification became unstable, which caused the turbulence intensification. From Fig. 8 it follows that the use of data measured during 5 min allows stable TEDR estimates to be derived and the evolution of the small-scale turbulence level to be observed with good resolution.

From data measured on 27 and 28 August 2003 we have retrieved 54 height profiles of TEDR, using both methods considered here (i.e., number of all profiles equals 2×54). Each profile is obtained from data measured during 5 min. It is obvious (see Fig. 4) that in Eqs. (51)–(59) the total number $N_s \times L$ of the corresponding parameters that are used for averaging is different for different heights h. For example, in the case of estimation of $\hat{\sigma}_t^2(h)$ or $\hat{D}_{\hat{V}_D}(r_i, h)$, where $r_i = 30$ m, at heights 0 m $\le h \le$ 250 m, the number $N_s \times L \approx 24\,000$ (the same number of estimates was used for the numerical simulation in section 2c), and at $h = 500$ m, $N_s \times L \approx 11\,000$. Because the number $N_s \times L$ is largest at low heights, the error of $\hat{\varepsilon}(h)$ estimation is increasing with height.

To draw reliable conclusions about the accuracy of the Doppler lidar TEDR measurements, it is necessary to compare the results of simultaneous (at the same

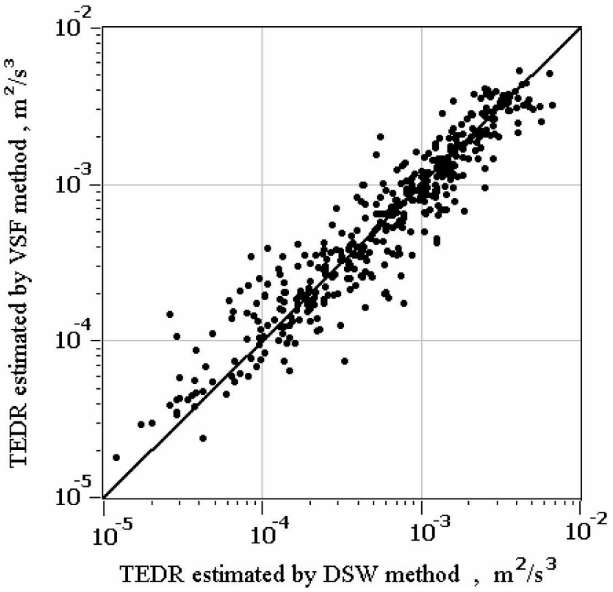

FIG. 9. Comparison of TEDR estimates obtained from VSF (y axis) and DSW (x axis) methods.

heights) measurements where the accuracy is known and is sufficiently high, for example, to compare with measurements from a set of sonic or cup anemometers mounted at different heights of a meteorological mast (Byzova et al. 1989). Because this possibility was not given, we compare the results of the measurement and numerical simulation.

For comparison of the TEDR estimates obtained by the VSF and DSW methods, all data measured on 27 and 28 August were used. Figure 9 shows the results of this comparison. It is seen that the points are located around the line of coincidence of the estimates. From the data of this figure we calculated the discrepancy parameter d given by Eq. (49), resulting in a value of $d = 41$ %.

In accordance with the simulation results shown in Fig. 3, the parameter $d \approx 25\%$ at $\varepsilon = 10^{-5}$ m^2 s^{-3}, and $d \approx 15\%$ at $\varepsilon > 10^{-4}$ m^2 s^{-3}. However, in the case of the real experiment the parameter $d = 41\%$ is ~1.5–2.5 times larger than the level of discrepancy for the estimates (by VSF and DSW methods) obtained from the simulated data. Therefore, the error of the TEDR measurements has to be also significantly larger than the theoretical results shown in Fig. 3.

Possible reasons for the discrepancy of the theoretical and experimental results (in relation to the TEDR measurement accuracy) consist of the following.

1) Geometrical factor

In the case of numerical simulation the estimates $\hat{V}_D$ and $\hat{\sigma}^2_{\text{sw}}$ are uniformly distributed on the area of 1200 m × 900 m (3 m s^{-1} × 300 s = 900 m). Because of the laser beam scanning, the estimates obtained from the measured data have a 3.4 times larger density at a 500-m range, as compared with the density at a 1700-m range. At a height of 500 m the sampling area within a layer of 50 m is approximately 2 times less than for heights $h \leq 250$ m (see Fig. 4). The exclusion of data affected by the wake vortices decreases the sampling area (not more than 10%). Except for a few cases (in particular, the last 20 min of measurements on 27 August), the mean wind velocity was not larger than 3 m s^{-1}. It is obvious, that the effective sampling area in the experiment is less than in the simulation.

2) Anisotropy and inhomogeneity of the wind field

In Eqs. (54), (57), and (58) we average the data measured at different elevation angles φ_l. Although in each layer of 50 m (gray belt in Fig. 4) the angle between the maximum and minimum elevation is relatively small (e.g., at $h = 200$ m it is $6^0 < \varphi_l < 27^0$), the anisotropy of large-scale turbulence variations is the reason for the inhomogeneity of the estimates $\hat{V}_D(R_k, \varphi_l)$ inside the layer. Therefore, in Eqs. (54), (57), and (58) we average the measured velocity with different integral scales of turbulence, and the model given by Eq. (33) can inadequately describe the measured data.

3) Other reasons

Other reasons that could explain the discrepancy of the theoretical and experimental results are the presence of mesoscale processes in the atmosphere and the fact that the probability density of the velocity difference is not Gaussian (in the inertial subinterval the third moment of the velocity difference $\sim\varepsilon$; Monin and Yaglom 1975). These two factors, as well as possible errors in measurement of σ_0^2 and $n_{\text{th}}^{\text{opt}}$ (especially for the case of weak turbulence) are not taken into account in the numerical simulation.

4. Conclusions

Two methods of TEDR estimation from data measured with the 2-μm pulsed Doppler lidar have been considered in this paper: the estimation from 1) the velocity structure function (VSF) and 2) the Doppler spectrum width (DSW). The data measured by scanning the laser beam in a vertical plane were used for estimation of the velocity structure function and the Doppler spectrum width. The algorithms for processing these data are described in detail.

The methods were applied for retrieving TEDR height profiles from lidar data acquired at the Tarbes-Lourdes-Pyrénées International Airport in summer 2003. The measurement geometry and the aircraft

flights over the airfield allowed information to be obtained about both the atmospheric turbulence and the aircraft wake vortices. From the data measured during 2 days of the experimental campaign 54 height profiles of TEDR were retrieved. Each set of profiles was derived by two estimation methods. In the mean, the results of TEDR estimation by the VSF and DSW methods are in good agreement. However, the discrepancy parameter d calculated from the experimental data equals 41%, and it is significantly larger than the simulation result (~25%–15%). Apparently, this is the consequence of different factors (listed in section 3b) that were not taken into account in the numerical simulation.

On the basis of the theoretical results shown in Figs. 2 and 3 we can draw the conclusion about the feasibilities of the VSF and DSW methods for TEDR estimation. For moderate and strong turbulence ($\varepsilon > 5 \times 10^{-4}$ m^2 s^{-3}) the accuracy of TEDR estimation from the Doppler spectrum width is 2 times higher than that in the case of the VSF method. The high sensibility of the DSW estimator to measurement errors of σ_0^2 and $n_{\text{th}}^{\text{opt}}$ in the case of weak turbulence can be the source of large errors for TEDR measurements. Therefore, for measurements at low turbulence level ($\varepsilon \leq 5 \times 10^{-4}$ m^2 s^{-3}) it is better to use the VSF method for TEDR estimation.

The accuracy of TEDR determination by the methods described in this paper is quite sufficient for the analysis of wake vortex behavior under different turbulent conditions (Köpp et al. 2005). An accuracy investigation of turbulence measurement with the pulsed Doppler lidar cannot be complete without intercomparison with measurement results of independent turbulence sensors.

Acknowledgments. The experimental part of the presented work has been carried out in the framework of the European research program AWIATOR (Contract G4RD-CT-2002-00836). The algorithms for data processing have been developed for the DLR project "Wirbelschleppe."

APPENDIX

List of Symbols and Acronyms

B	Spectral bandwidth
$B_V(r)$	Correlation function of the wind velocity
$C_K \approx 2$	Kolmogorov constant
$D_V(r)$	Structure function of the wind velocity
$D_{\hat{V}_D}(r)$	Structure function of the Doppler lidar estimate of the radial velocity
$D_{V_D}(r)$	Structure function of the radial wind velocity averaged over the sensing volume
$D_e(r)$	Structure function of random error of the velocity estimation
DSW	Method of TEDR estimation from Doppler spectrum width
$e(R)$	Random error of the velocity estimation
$E(R)$	Random error of the Doppler spectrum width estimation
$J_B^{(i)}(mT_s)$	Backscatter signal
$J_M^{(i)}(mT_s)$	Monitor signal
L	Number of estimates in a layer of 50-m thickness at one scan
L_o	Outer scale of turbulence
L_V	Integral scale of turbulence
N_a	Number of shots used for spectral accumulation
N_s	Number of scans used for averaging
n_{th}	Noise threshold used for estimation of the Doppler spectrum parameters
$\hat{P}_s(R)$	Estimate of the normalized signal power
$P_M(t)$	Monitor signal power
PRF	Pulse repetition frequency
$Q_s(z)$	Function characterizing the spatial averaging over the sensing volume
R	Range (distance between lidar and center of the sensing volume)
$\hat{S}_D^{(i)}(\Delta fk, R)$	Signal power spectrum (or Doppler spectrum) estimate obtained from data of ith shot
$\tilde{S}_D(\Delta fk, R)$	Estimate of Doppler spectrum after accumulation and normalization
$S_D(f, R)$	Doppler spectrum estimate averaged over all random parameters except the radial wind velocity
$S'_D(f, R)$	Doppler spectrum estimate fluctuations
SNR	Signal-to-noise ratio: ratio of mean signal power to mean noise power within the spectral bandwidth of 50 MHz
$S_V(\kappa)$	Spatial wind velocity spectrum
T_s	Sampling interval (2 ns)
T_{eff}	Effective time of Doppler spectrum measurement (one shot)
U_p	Pulse energy
V_c	Crosswind velocity
$\hat{V}_D(R)$	Doppler lidar estimate of the radial velocity
$V_D(R)$	Radial wind velocity averaged over the sensing volume
$V_r(z)$	Radial wind velocity at point z
VSF	Method of TEDR estimation from the velocity structure function
$W(m'T_s)$	Window function

δf	Intermediate frequency
Δf	Frequency bin width
Δf_r	Frequency resolution
Δz	Longitudinal size of the sensing volume
ε	Turbulent energy dissipation rate
$\hat{\varepsilon}_1$	TEDR estimated from the VSF
$\hat{\varepsilon}_2$	TEDR estimated from the DSW
λ	Laser wavelength
$\mu(R)$	Wind shear
σ_e^2	Variance of random error of the velocity estimation
$\hat{\sigma}_f^2$	Estimate of square of the Doppler spectrum width
σ_δ^2	Variance of the intermediate frequency
σ_0	Doppler spectrum width in the case of homogeneous wind
σ_s	Doppler spectrum broadening resulting from wind shear
σ_t	Doppler spectrum broadening resulting from turbulence
$\sigma_u(R)$	Doppler spectrum broadening resulting from inhomogeneity of the wind inside the sensing volume
σ_{Mf}	Width of the monitor signal power spectrum
σ_p	Pulse duration
σ_V^2	Wind velocity variance
$\sigma_{V_D}^2$	Variance of the Doppler lidar estimate of the radial velocity
$\sigma_{V_D}^2$	Variance of the radial wind velocity averaged over the sensing volume
σ_W	Width of the Gaussian window
φ	Elevation angle
$\hat{X}$	Estimate of X
$\langle X \rangle$	Ensemble averaging of X
$\langle X \rangle_E$	Estimate of the mean of X (using spatial and temporal averaging)

REFERENCES

Banakh, V. A., and I. N. Smalikho, 1997: Estimation of the turbulent energy dissipation rate from the pulsed Doppler lidar data. *Atmos. Oceanic Opt.,* **10,** 957–965.

——, ——, F. Köpp, and Ch. Werner, 1995: Representativeness of wind measurements with a cw Doppler lidar in the atmospheric boundary layer. *Appl. Opt.,* **34,** 2055–2067.

——, ——, ——, and ——, 1999: Measurements of turbulent energy dissipation rate with a cw Doppler lidar in the atmospheric boundary layer. *J. Atmos. Oceanic Technol.,* **16,** 1044–1061.

Brockman, P. B., C. Barker, G. J. Koch, D. P. C. Nguyen, and C. L. Britt, 1999: Coherent pulsed lidar sensing of wake vortex position and strength, winds and turbulence in the thermal area. *Proc. 10th Coherent Laser Radar Technology and Applications Conf.*, Mount Hood, OR, 12–15.

Byzova, N. L., V. N. Ivanov, and E. K. Garger, 1989: *Turbulence in the Boundary Layer of the Atmosphere.* Gidrometeoizdat, 262 pp.

Cal-Chen, T., M. Xu, and W. L. Eberhard, 1992: Estimation of atmospheric boundary layer fluxes and other turbulence parameters from Doppler lidar data. *J. Geophys. Res.,* **97,** 18 409–18 423.

Constant, G., R. Foord, P. A. Forrester, and J. M. Vaughan, 1994: Coherent laser radar and the problem of aircraft wake vortices. *J. Mod. Opt.,* **41,** 2153–2173.

Davies, F., C. G. Collier, G. N. Pearson, and K. E. Bozier, 2004: Doppler lidar measurements of turbulent structure function over an urban area. *J. Atmos. Oceanic Technol.,* **21,** 753–761.

Eberhard, W. L., R. E. Cupp, and K. R. Healy, 1989: Doppler lidar measurements of profiles of turbulence and momentum flux. *J. Atmos. Oceanic Technol.,* **6,** 809–819.

Frehlich, R., 1997: Effect of wind turbulence on coherent Doppler lidar measurements. *J. Atmos. Oceanic Technol.,* **14,** 54–75.

——, 2001: Estimation of velocity error for Doppler lidar measurements. *J. Atmos. Oceanic Technol.,* **18,** 1628–1639.

——, and L. Cornman, 1999: Coherent Doppler lidar signal spectrum with wind turbulence. *Appl. Opt.,* **38,** 7456–7466.

——, and ——, 2002: Estimating spatial velocity statistics with coherent Doppler lidar. *J. Atmos. Oceanic Technol.,* **19,** 355–366.

——, S. M. Hannon, and S. W. Henderson, 1994: Performance of a 2-μm coherent Doppler lidar for wind measurements. *J. Atmos. Oceanic Technol.,* **11,** 1517–1528.

——, S. M. Hannon, and S. W. Henderson, 1998: Coherent Doppler lidar measurements of wind field statistics. *Bound.-Layer Meteor.,* **86,** 233–256.

Gerz, T., F. Holzäpfel, and D. Darracq, 2002: Commercial aircraft wake vortices. *Prog. Aerosp. Sci.,* **38,** 181–202.

Gordienko, V. M., A. A. Kormakov, L. A. Kosovsky, N. N. Kurochkin, G. A. Pogosov, A. V. Priezzhev, and Y. Y. Putivskii, 1994: Coherent CO_2 lidars for measuring wind velocity and atmospheric turbulence. *Opt. Eng.,* **33,** 3206–3213.

Hall, F. F., R. M. Huffaker, R. M. Hardesty, M. E. Jackson, T. R. Lawrence, M. J. Post, R. A. Richter, and B. F. Weber, 1984: Wind measurement accuracy of the NOAA pulsed infrared Doppler lidar. *Appl. Opt.,* **23,** 2503–2506.

Hannon, S. M., and J. A. Thomson, 1994: Aircraft wake vortex detection and measurement with pulsed solid-state coherent laser radar. *J. Mod. Opt.,* **41,** 2175–2196.

Harris, M., J. M. Vaughan, K. Huenecke, and C. Huenecke, 2000: Aircraft wake vortices: A comparison of wind-tunnel data with field-trial measurements by laser radar. *Aerosp. Sci. Technol.,* **4,** 363–370.

——, R. I. Young, F. Köpp, A. Dolfi, and J.-P. Cariou, 2002: Wake vortex detection and monitoring. *Aerosp. Sci. Technol.,* **6,** 325–331.

Hawley, J. G., R. Tang, S. W. Henderson, C. P. Hale, M. J. Kavaya, and D. Moerder, 1993: Coherent launch-site atmospheric wind sounder: Theory and experiment. *Appl. Opt.,* **32,** 4557–4567.

Henderson, S. W., P. J. M. Suni, C. P. Hale, S. M. Hannon, J. R. Magee, D. L. Bruns, and E. H. Yuen, 1993: Coherent laser radar at 2 μm using solid-state lasers. *IEEE Trans. Geosci. Remote Sens.,* **31,** 4–15.

Hildebrand, P. H., and R. S. Sekhon, 1974: Objective determination of the noise level in Doppler spectra. *J. Appl. Meteor.,* **13,** 808–811.

Holzäpfel, F., 2003: Probabilistic two-phase wake vortex decay and transport model. *J. Aircr.,* **40,** 323–331.

——, and R. E. Robins, 2004: Probabilistic two-phase aircraft wake-vortex model: Application and assessment. *J. Aircr.,* **41,** 1–10.

——, T. Gerz, and R. Baumann, 2001: The turbulent decay of trailing vortex pairs in stably stratified environments. *Aerosp. Sci. Technol.,* **5,** 95–108.

——, T. Hofbauer, D. Darracq, H. Moet, F. Garnier, and C. Ferreira Gago, 2003: Analysis of wake vortex decay mechanisms in the atmosphere. *Aerosp. Sci. Technol.,* **7,** 236–275.

Keane, M., D. Buckton, M. Redfern, C. Bollig, C. Wedekind, F. Köpp, and F. Berni, 2002: Axial detection of aircraft wake vortices using Doppler lidar. *J. Aircr.,* **39,** 850–862.

Keeler, R. J., R. J. Serafin, R. L. Schwiesow, D. H. Lenschow, J. M. Vaughan, and A. A. Woodfield, 1987: An airborne laser air motion sensing system. Part I: Concept and preliminary experiment. *J. Atmos. Oceanic Technol.,* **4,** 113–127.

Köpp, F., 1994: Doppler lidar investigation of wake vortex transport between closely spaced parallel runways. *AIAA J.,* **32,** 805–810.

——, 1999: Wake-vortex characteristics of military-type aircraft measured at airport Oberpfaffenhofen using the DLR laser Doppler anemometer. *Aerosp. Sci. Technol.,* **3,** 191–199.

——, R. L. Schwiesow, and Ch. Werner, 1984: Remote measurements of boundary-layer wind profiles using a CW Doppler lidar. *J. Climate Appl. Meteor.,* **23,** 148–154.

——, and Coauthors, 2003: Characterisation of aircraft wake vortices by multiple-lidar triangulation. *AIAA J.,* **41,** 1081–1088.

——, S. Rahm, and I. N. Smalikho, 2004: Characterization of aircraft wake vortices by 2-μm pulsed Doppler lidar. *J. Atmos. Oceanic Technol.,* **21,** 194–206.

——, ——, ——, A. Dolfi, J.-P. Cariou, M. Harris, and R. I. Young, 2005: Comparison of wake-vortex parameters measured by pulsed and continuous-wave lidars. *J. Aircr.,* **42,** 916–923.

Lumley, J. L., and H. A. Panofsky, 1964: *The Structure of Atmospheric Turbulence.* Willey-Interscience, 264 pp.

Monin, A. S., and A. M. Yaglom, 1975: *Mechanics of Turbulence.* Vol. 2, *Statistical Fluid Mechanics,* The MIT Press, 874 pp.

Reitebuch, O., Ch. Werner, I. Leike, P. Delville, P. Flamant, A. Cress, and D. Engelbart, 2001: Experimental validation of wind profiling performed by the airborne 10-μm heterodyne Doppler lidar WIND. *J. Atmos. Oceanic Technol.,* **18,** 1331–1344.

Salamitou, P., A. Dabas, and P. H. Flamant, 1995: Simulation in the time domain for heterodyne coherent laser radar. *Appl. Opt.,* **34,** 499–506.

Smalikho, I. N., 1995: On measurement of the dissipation rate of turbulent energy with a cw Doppler lidar. *Atmos. Oceanic Opt.,* **8,** 788–793.

——, 1997: Accuracy of turbulent energy dissipation rate estimation from wind velocity temporal spectrum. *Atmos. Oceanic Opt.,* **10,** 898–904.

——, 2003: Techniques of wind vector estimation from data measured with a scanning coherent Doppler lidar. *J. Atmos. Oceanic Technol.,* **20,** 276–291.

Vaughan, J. M., and M. Harris, 2001: Lidar measurement of B747 wakes: Observation of a vortex within a vortex. *Aerosp. Sci. Technol.,* **5,** 409–411.

Vinnichenko, N. K., N. Z. Pinus, S. M. Shmeter, and G. N. Shur, 1973: *Turbulence in the Free Atmosphere.* Consultant Bureau, 263 pp.

Werner, Ch., and Coauthors, 2001: Wind infrared Doppler lidar instrument. *Opt. Eng.,* **40,** 115–125.